Eur. Phys. J. E **28**, 401–409 (2009)
DOI 10.1140/epje/i2008-10434-0

THE EUROPEAN PHYSICAL JOURNAL E

Regular Article

Collective alignment of polar filaments by molecular motors

F. Ziebert[1,2,a], M. Vershinin[3], S.P. Gross[3], and I.S. Aranson[1]

[1] Argonne National Laboratory - 9700 South Cass Avenue, Argonne, IL 60439, USA
[2] Laboratoire de Physico-Chimie Théorique - UMR CNRS Gulliver 7083, ESPCI, 10 rue Vauquelin, F-75231 Paris, France
[3] Department of Developmental and Cell Biology - University of California-Irvine, Irvine, CA, USA

Received 13 May 2008 and Received in final form 14 January 2009
Published online: 27 March 2009 –

Abstract. We study the alignment of polar biofilaments, such as microtubules and actin, subject to the action of multiple molecular motors attached simultaneously to more than one filament. Focusing on a paradigm model of only two filaments interacting with multiple motors, we were able to investigate in detail the alignment dynamics. While almost no alignment occurs in the case of a single motor, the filaments become rapidly aligned due to the collective action of the motors. Our analysis shows that the alignment time is governed by the number of bound motors and the magnitude of the motors' stepping fluctuations. We predict that the time scale of alignment is in the order of seconds, much faster than that reported for passive crosslink-induced bundling. *In vitro* experiments on the alignment of microtubules by multiple-motor covered beads are in qualitative agreement. We also discuss another mode of fast alignment of filaments, namely the cooperation between motors and passive crosslinks.

PACS. 87.16.-b Subcellular structure and processes – 05.65.+b Self-organized systems – 87.16.Nn Motor proteins (myosin, kinesin dynein)

1 Introduction

The fascinating self-organizing behavior of polar biofilaments such as microtubules and F-actin, that form the cytoskeleton of the majority of living cells, continues to attract attention both among biologists and physicists. Recent experimental studies revealed a variety of self-organized structures like three-dimensional active gels, two-dimensional networks occurring underneath the cell membrane, aster-like patterns similar to that formed during mitosis, as well as one-dimensional bundle structures found *e.g.* in stress fibers. While *in vivo* these structures are controlled by a plethora of proteins and signaling pathways [1], it has been established [2–6] that such structures are also formed *in vitro*, in the absence of regulatory proteins and signaling pathways. In turn, the structure formation as well as the nonequilibrium response of motor-activated gels composed of biofilaments has also become an active field of theoretical research [7–9].

Bundles of polar biofilaments such as F-actin and microtubules play an important role in the cytoskeleton's functioning and elasticity. Bundle contraction has been investigated [10–12] as well as bundle elasticity [13,14], however the dynamics of bundle formation is not well understood. There are situations, *e.g.* when the filaments are growing from organizing centers in a specified direction, where the regulation and the confined geometry lead to bundling. On the other hand, *in vitro* experiments [15] showed that passive crosslinks can induce bundling, and such a transition for nearly parallel semiflexible filaments has been discussed theoretically [16]. Crosslink-induced bundling is rather slow, since this mechanism relies on diffusion. However, it is generally believed that linear molecular motors like kinesin or myosin, which convert chemical energy from adenosine triphosphate (ATP) hydrolysis into directed mechanical motion, play an important role in the alignment of individual filaments, which can be considered as a precursor of bundle formation. Practically nothing is known about the dynamics of bundle organization due to motor activity and about the relevant parameters (*e.g.* motor concentration, processivity, etc.) determining the characteristic time of the alignment.

In this work we predict analytically and demonstrate by *in vitro* experiments that filaments become aligned due to the collective action of multiple motors. Taking advantage of a highly simplified yet nontrivial micromechanical model containing only two filaments interacting with multiple motors, we were able to investigate in detail the dynamics of the filaments' alignment (or zipping in the terminology of Ref. [17]). Both theory and experiment revealed that the polar filaments become aligned on a time scale of several seconds due to collective action of

[a] e-mail: fziebert@turner.pct.espci.fr

many motors. This scale is faster by two orders of magnitude than the alignment time by passive crosslinks (several minutes) reported, *e.g.*, in reference [15]. This fast alignment is a collective effect, since a single motor, even if it is a highly processive one, is known to lead to practically no alignment [8]. Our model also indicates that the alignment time is related to the number of attached motors and the stochastic nature of motor motion: the alignment time is directly related to the randomness in the motor stepping and force. A second important situation, discussed theoretically in this work, is the cooperation between mobile motors and stationary crosslinks. In this case, a single motor-crosslink pair is sufficient for fast alignment.

The structure of the paper is the following. In Section 2 we propose a simplified model for two rigid rods interacting with multiple motors and discuss in detail the assumptions made. Results of molecular dynamics simulations for rigid and semiflexible filaments are presented in Section 3. In Section 4 we present an analytical solution of our model in the continuum limit and estimates for the corresponding alignment time. The case of a single motor-crosslink pair is studied in Section 5. In Section 6 we present results of *in vitro* experiments on the alignment of microtubule pairs by kinesin-covered nanobeads. Conclusions and a discussion are presented in Section 7.

2 Model

To investigate the alignment of polar filaments by multiple motors, we focus on the simplest situation of a pair of two perfectly rigid rods of fixed length L interacting with molecular motors attached to both rods. We consider either motor oligomers with multiple heads, as used in references [4–6,18], or multiple motors attached to polystyrene nanobeads as in reference [19]. The motors are modeled by massless linear springs attached perpendicular to the bisector, see Figure 1. Due to the great disparity in the sizes of biofilaments and molecular motors ($\simeq$ 10–20 μm *vs.* $\simeq$ 100 nm), the marching of a motor attached to only *one* filament produces no noticeable displacement of the filament. Thus we can restrict ourselves to motors attached to both filaments. This remains true as long as one considers motor-covered beads of small size ($\simeq$ 200 nm), as in the experimental demonstration in Section 6.

The number of attached motors, N, is not fixed: the motors can attach to both filaments, at the intersection point of the two rods, with a probability p_a, as well as detach from any place with a fixed detachment rate p_d. A more detailed description of the kinetics, where motors attach to a single microtubule first and then, upon marching close to the intersection point, attach to the second microtubule, only renormalizes the corresponding attachment rate. As a further simplification, we focus on the symmetric case, *i.e.* the distance S_0 (with $-L/2 < S_0 < L/2$) of the intersection point from the center of mass of the tubules is the same for both motor heads. Then the force exerted on the filament pair by the motor is perpendicular to the bisector of the angle between the tubules, *i.e.* parallel to the Y-axis (see Fig. 1). It is easy to see that if motors

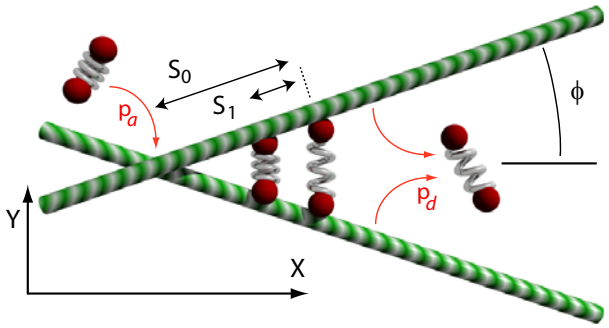

Fig. 1. Sketch of two microtubules interacting with multiple motors. Motors attach with a probability p_a at the intersection point S_0, move along the tubules (in $+X$ direction) while exerting a spring-like force, and detach with a rate p_d.

attach asymmetrically to both rods, the latter will soon assume a symmetric position, as discussed in [8]. Namely, if the motor attaches asymmetrically, the leading motor head (corresponding to larger distance S_0 from the center) is slowed down by the force due to extension of the motor's spring whereas the trailing head is accelerated, leading to a fast relaxation towards a symmetric configuration. Finally, most experiments take place in a quasi-two-dimensional geometry (*e.g.* shallow microchambers). Moreover, if several motors are attached to the filaments, the latter are kept approximately within a plane. Thus we restrict ourselves to the two-dimensional case. However, in view of the situation in biological cells, a generalization to a full three-dimensional version of the model, with two independent angles and accounting for out-of-plane torque, is rather straightforward.

The equations of motion for the rod-like filaments follow from the balance of forces and torques exerted on the rods by the motors and the environment (viscous drag). The torque balance leads to an equation for the intersection angle ϕ, as defined in Figure 1

$$\eta_r \dot{\phi} = \tau, \tag{1}$$

where $\eta_r \simeq \frac{\pi\eta L^3}{3\ln(L/b)}$ is the rotational friction coefficient [20], b is the rod diameter and η is the fluid viscosity. Neglecting the motors' bending rigidity, the force of the n-th motor, F_n, acts exactly along the Y-axis, see Figure 1. The total torque τ created by the motor forces F_n and the drag force then reads $\tau = \sum F_n S_n \cos\phi$, with S_n the position of the n-th motor. The motor force F_n is described by a linear spring, $F_n = -\kappa l$, where κ is the motor's spring constant and $l = (S_n - S_0)\sin\phi$ is the spring extension. S_0 is the position of the intersection point of the two tubules, see again Figure 1. Finally we arrive at the torque balance

$$\dot{\phi} = \frac{\kappa}{\eta_r}\cos\phi\sin\phi\sum_{n=1}^{N} S_n(S_0 - S_n). \tag{2}$$

For the stepping dynamics of the n-th motor we write

$$\dot{S}_n = V\left[1 - \kappa(S_n - S_0)\sin^2\phi/F_{st}\right] + \xi_n(t). \tag{3}$$

Here we have used a well-accepted linear force-velocity relation [21,22] of the form

$$V(F) = V(1 - F_n^{\parallel}/F_{st}). \tag{4}$$

Therein V is the motor velocity without load and F_{st} is the stall force (forward motion of the motor is impossible above stall force). $F_n^{\parallel}$ is the force F_n opposing the motor motion projected on the direction of the rod. The stochastic term ξ_n describes random fluctuations in the stepping and force of the motor. We assume

$$\langle \xi_n(t) \rangle = 0$$

and

$$\langle \xi_n(t)\xi_m(t') \rangle = 2D\delta(t-t')\delta_{nm}. \tag{5}$$

The noise strength D resulting from the fluctuations in the stepping dynamics of motors can be estimated from available experimental measurements of the so-called "randomness parameter" [23]. This parameter relates the motor's velocity V with the noise strength D (or the motor's diffusivity) and is defined as

$$r = \lim_{t\to\infty} \frac{\langle x(t)^2 \rangle - \langle x(t) \rangle^2}{d\langle x(t) \rangle} = \frac{2D}{dV}\,. \tag{6}$$

Here $d = 8\,\mathrm{nm}$ is the motor step size. From reference [23] we deduce $r \simeq 0.4$, which results for $V \simeq 0.2\,\mu\mathrm{m/s}$ in the estimate $D \simeq 3 \cdot 10^{-4}\,\mu\mathrm{m}^2/\mathrm{s}$.

Before proceeding, we would like to illustrate a nontrivial effect: Equations (3) imply an *effective attraction* between the motors. Indeed, in the absence of noise, any difference in the attachment positions $S = S_i - S_j$ follows

$$\mathrm{d}S/\mathrm{d}t = -V\kappa S \sin^2\phi/F_{st}. \tag{7}$$

One sees immediately from equation (7) that the distance S always decreases since $\mathrm{d}S/\mathrm{d}t/S = -V\kappa \sin^2\phi/F_{st} \leq 0$. This effect has a simple interpretation: the spring of the leading motor ($S_i > S_j$) is more stretched and thus experiences a larger opposing force than the trailing one. According to the force-velocity relation, equation (4), the leading motor will move slower than the trailing one, and the distance between them will decrease. Thus, equations (3) describe two competing processes: localization of the motor distribution near the intersection point due to the effective attractive interaction between the motors and spreading of the distribution due to the random force ξ.

To close the description we need a dynamic equation for the intersection point of the rods. We denote with x_0, y_0 the coordinates of the center of mass of the upper microtubule in Figure 1 with respect to the intersection point. Then an equation for the intersection point can be achieved from the geometrical constraint $y_0 = -S_0 \sin\phi$ and the equation of motion for the center of mass of the tubules, $\eta_t \dot{y}_0 = F_d$. Here $F_d = \sum F_n$ is the viscous drag force and $\eta_t \simeq \eta_\perp = \frac{4\pi\eta L}{\ln(L/b)}$ the translational friction coefficient [20]. For simplicity we have neglected the anisotropy of the translational friction by letting $\eta_\parallel = \eta_\perp = \eta_t$. This results in $\partial_t x_0 = 0$, *i.e.* there is no overall translation of the center of mass. Finally, the equation for the intersection point coordinate S_0 is

$$\dot{S}_0 = -\kappa \sum_{n=1}^{N} \left(\frac{\cos^2\phi S_0}{\eta_r} S_n(S_0 - S_n) + \frac{S_0 - S_n}{\eta_t} \right). \tag{8}$$

Above we proposed a model with fixed rates p_a and p_d for the attachment/detachment kinetics. It is however known that the detachment rate is in fact force-dependent [24]. The approximate dependence, consistent with experiments, reads [25,26]

$$p_d = p_0 \exp\left(\frac{\kappa a l}{k_B T}\right). \tag{9}$$

Here p_0 is the detachment rate without opposing force, a is a molecular length scale (a few nm) and l is again the extension of the motor. The argument in the exponential is the ratio of the stretching energy of the motor and the thermal energy; the higher the force acting on the motor, the higher the probability of detachment. For completeness, this important feature of the motor's kinetics has also been included in the model.

3 Numerical results

Equations (2, 3) and (8) with both attachment/detachment kinetics (with or without force dependence) can be solved by a standard Langevin scheme. For this purpose the noise terms in equations (3) were implemented as $\xi_n(t_i) = \zeta\Delta$, where $\zeta \in (-\frac{1}{2}, \frac{1}{2})$ is a random number drawn for every attached motor and at every time step t_i from a uniform distribution. The amplitude of the noise is $\Delta = \sqrt{24D\mathrm{d}t}$, with $\mathrm{d}t$ the time increment, to fulfill equations (5). At each time step, additional random numbers were generated for the detachment of already present motors and the attachment of new ones, according to the rates defined above. Parameters have been chosen in the ranges of the following known or estimated values: kinesin velocity $V = 0.01$–$1\,\mu\mathrm{m/s}$ (depending on the ATP concentration) [23]; kinesin spring constant $\kappa = 200$–$400\,\mathrm{pN}/\mu\mathrm{m}$ [27]; stall force of kinesin $F_{st} = 5$–$8\,\mathrm{pN}$ [23]; attachment/detachment rates of order $p_a \sim 10\,\mathrm{s}^{-1}$ and $p_d \sim 1\,\mathrm{s}^{-1}$ [28]; solvent viscosity $\eta \sim 0.005\,\mathrm{pNs}/\mu\mathrm{m}^2$; microtubule length $L = 10$–$15\,\mu\mathrm{m}$, and diameter $b = 24\,\mathrm{nm}$.

Figure 2 shows select numerical results for the angle ϕ between the tubules evolving in time due to the collective action of motors. The black line was obtained by the model with a constant motor velocity V, *i.e.* without any force dependence of the motor speed or the detachment rate (limit of infinite stall force F_{st}). As one sees from Figure 2, alignment (zipping) occurs on a time scale of a few seconds. For comparison, Figure 2 also shows results taking into account the force-dependent effects: the red line has been obtained with the force-velocity relation, equation (4). For the green line a force-dependent detachment rate, equation (9), has been implemented. Finally the blue line displays the behavior for both force-dependent effects

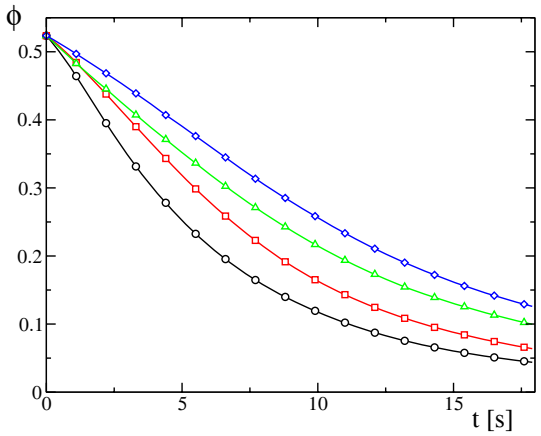

Fig. 2. (Color online) The angle ϕ *vs.* time t during the motion of multiple motors. Black line (○): simplest model without force-dependent effects. The angle decreases rapidly, *i.e.* the motors zipper the microtubules. Red line (□): with force-velocity dependence. Green line (△): with force-dependent detachment rate. Blue line (◇): with both. Obtained by Langevin simulations with $D = 10^{-4}\,\mu\text{m}^2/\text{s}$, $V \simeq 0.2\,\mu\text{m/s}$, $p_a = 10\,\mu\text{m/s}$, $p_d = 1/\text{s}$; initial conditions $\phi(t=0) = \pi/6$, $S_0(t=0) = 0$, averaged over 500 runs.

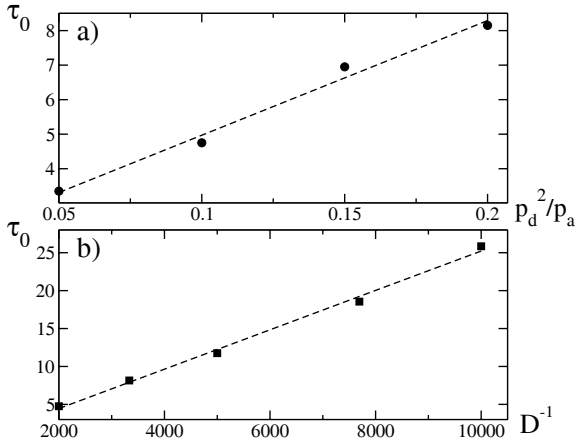

Fig. 3. Dependence of the characteristic alignment time τ_0 on the motor kinetics, p_a and p_d (panel a), and on the inverse fluctuation strength D^{-1} (panel b). The alignment time is linear in both chosen parameter combinations, $\tau_0 \propto p_d^2/p_a$ and $\tau_0 \propto 1/D$. Obtained by Langevin simulations with $V \simeq 0.2\,\mu\text{m/s}$; $D = 10^{-4}\,\mu\text{m}^2/\text{s}$ for panel a) and $p_a = 10\,\mu\text{m/s}$, $p_d = 1/\text{s}$ for panel b).

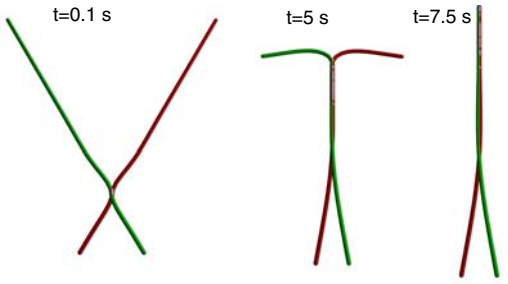

Fig. 4. Three snapshots illustrating the effect of actin-like flexibility (bending stiffness $\beta = 0.073\,\text{pN}\,\mu\text{m}^2$) on the alignment induced by multiple motors. The finite flexibility increases the alignment time only by a factor of 2-3 compared to perfectly rigid filaments, although some buckling occurs.

together. As one can see, both force-dependent effects lead to slower zipping and are approximately additive. However, for the relevant range of model parameters both effects lead only to quantitative changes in the alignment behavior.

Thus, if we restrict ourselves to the simplest case (*i.e.* without force-dependent effects), Figure 3 shows the numerically obtained dependences of the characteristic alignment time τ_0 on the motor's detachment/attachment rates and on the fluctuation strength D. As one sees, for not too large angles (again $\phi(t=0) = \pi/6$ has been used for this figure), apparently $\tau_0 \propto p_d^2/p_a$ and $\tau_0 \propto 1/D$ and thus both an increase in the average number of motors ($\propto p_a/p_d$) and in the fluctuation strength lead to faster zipping.

We have also investigated the effect of filament flexibility, *i.e.* finite bending stiffness, by Brownian dynamics simulations similar to those in reference [29]. Two filaments were represented by two-dimensional space curves $\mathbf{r}(s)$ (parameterized by the arclength s) and then discretized. All the implications of equations (2, 3) and (8) could be implemented for this generalized situation. In addition, we included the bending force $\mathbf{F}_b = -\beta\partial_s^4\mathbf{r}(s)$, with β the bending stiffness.

Multiple motors induced fast and effective zipping for both stiff and semiflexible filaments. To test the effect of finite flexibility, we used a value of $\beta = 0.073\,\text{pN}\mu\text{m}^2$ as reported for actin [30]. Figure 4 shows select results for such actin-like bending stiffness. The alignment is only slower by a factor of 2-3 as compared to perfectly stiff rods, although some filament buckling similar to that reported in reference [31] occurs. Thus, one can conclude that finite flexibility does not lead to qualitative changes in the time scales of alignment. Whether buckling occurs depends on the stepping fluctuations D: it occurs for low randomness values (as for the value $D = 10^{-4}\,\mu\text{m}^2/\text{s}$ used to obtain Fig. 4), while it is suppressed for large randomness.

4 Continuum description and alignment time

To understand the time scale associated with the alignment process, it is useful to consider a continuum limit that allows for an analytical treatment. From equation (3) one can derive the Fokker-Planck equation [32] for the probability distribution function $P(S,t)$ to find a motor at position S at time t, which reads

$$\partial_t P = D\partial_S^2 P - \partial_S(\tilde{V}P) - p_d P + p_a\delta(S - S_0(t)), \quad (10)$$

with the drift velocity, cf. equation (4),

$$\begin{aligned}\tilde{V} &= \tilde{V}(S - S_0(t)) \\ &= V\left[1 - \kappa(S - S_0(t))\sin^2\phi/F_{st}\right]. \end{aligned} \quad (11)$$

The different contributions on the right-hand side of equation (10) are diffusion by fluctuations in the motor steps, drift by the motors' marching with force-dependent velocity $\tilde{V}$, detachment of motors from any position, and finally attachment of motors. In the last term, the δ-function ensures attachment at the intersection point S_0 only.

Equations for the angle ϕ and the intersection point S_0 can be obtained by taking the continuum limit of equations (2) and (8), resulting in [33]

$$\dot{\phi} = \frac{\kappa}{\eta_r} \cos\phi \sin\phi \int_{-L/2}^{L/2} \mathrm{d}S P(S) S (S_0 - S), \tag{12}$$

$$\dot{S}_0 = -\kappa \int_{-L/2}^{L/2} \mathrm{d}S P(S)(S_0 - S) \left(\frac{\cos^2\phi S_0}{\eta_r} S + \frac{1}{\eta_t} \right). \tag{13}$$

Equations (10–13) can be solved analytically if one assumes that the attachment/detachment kinetics is sufficiently fast compared to the relative displacement of the motors and the intersection point, *i.e.* $p_d \gg V/L$. Then the motor distribution $P(S)$ is slowly varying in the frame moving along with the intersection point, *i.e.* $P(S,t) = P(S - S_0(t))$. Introducing $\tilde{S} = S - S_0(t)$, one obtains a quasi-stationary problem from equation (10),

$$0 = D\partial_{\tilde{S}}^2 P - (\delta V - \alpha \tilde{S})\partial_{\tilde{S}} P - (p_d - \alpha) P + p_a \delta(\tilde{S}), \tag{14}$$

with $\delta V = V - \dot{S}_0$ and $\alpha = V\kappa \sin^2\phi / F_{st}$.

Equation (14) can be solved exactly in the absence of the force-dependent effects described by equations (4, 9). This is the case when the motor forces are much smaller than the stall force, $F/F_{st} \to 0$. One obtains exponential solutions on both sides of the intersection point $\tilde{S} = 0$, that have to be matched at $\tilde{S} = 0$. Details of the calculations can be found in Appendix A. In case of a load-dependent motor speed, equation (4), the homogeneous part of equation (14) has an analytical solution in terms of confluent hypergeometric functions. Since this solution is impractical to proceed with, we obtained approximate solutions for not too high values of α, see Appendix A. Force-dependent detachment leads to a solution in terms of Bessel functions. Finally, since the motors are closely concentrated around the intersection point, the effects of both force dependences are corrections to the force-independent case and do not lead to changes in qualitative behavior.

Having obtained the distribution function $P(S)$ of the motors, the integrals in equations (12, 13) for the angle and the intersection point can be evaluated analytically. Keeping only terms in linear order in the small variable δV, cf. Appendix A, the effect of the motion of multiple motors on a pair of microtubules can be described by a *single* equation for the mutual angle ϕ (as defined in Fig. 1)

$$\dot{\phi} = -\cos\phi \sin\phi \frac{\bar{\eta}(V S_0 + 2D\frac{\kappa}{\eta_t} f)}{1 + \bar{\eta}\cos^2\phi S_0^2}. \tag{15}$$

Here we used the abbreviation $S_0 = S_0(t) = S_i + Vt$ for the position of the intersection point, with initial position $S_i = S_0(t=0)$. We also introduced the relative frictional coefficient $\bar{\eta} = \eta_t/\eta_r$.

Remarkably, equation (15) captures both the single-motor as well as the multiple-motor case: The case of a single motor interacting with two rigid rods had been discussed already in reference [8]. As detailed there, the evolution of the angle between the two filaments is described by

$$\dot{\phi} = -\cos\phi \sin\phi \frac{\bar{\eta} V S_0}{1 + \bar{\eta}\cos^2\phi S_0^2}. \tag{16}$$

As one sees, the single-motor case is recovered from equation (15) by setting the parameter $f = 0$. This parameter thus incorporates the collective effects of the motors: For multiple motors, $f = p_a/p_d^2$ holds in case of a force-independent motor speed. If the force-velocity relation, equation (4), is taken into account, f becomes a rather complicated function of the angle [34], to leading order

$$f = \frac{p_a}{p_d^2} \left(1 - 2\frac{V\kappa \sin^2\phi}{p_d F_{st}} \right). \tag{17}$$

From this formula one can see that the force dependence of the velocity reduces the collective effect ($f < \frac{p_a}{p_d^2}$). This correction is however small for small angles.

Let us discuss equation (15) in detail. For a single motor ($f = 0$) the change in the angle is totally due to the motion of the intersection point —where the single motor has to be located— and is governed by the term VS_0 in equation (15). In this case, the angle decreases only if the intersection point is on the right side with respect to the center of rod ($S_0 > 0$), while increasing if at the opposite side ($S_0 < 0$). A global (averaged) reduction in the mutual angles is thus a purely statistical effect, *i.e.* only occurs upon averaging over many realizations of intersection points/motor positions [8]. In contrast, in the case of multiple motors, there is the second term $\sim f$, which represents the collective effects and is proportional to the average number of motors and the fluctuation strength. This term always adds a negative contribution and thus reduces the angle. If this term dominates, there is fast alignment. For not too high mutual angles ϕ, this remains true when load dependence and/or force-dependent detachment rate, given by equations (4, 9), are considered. These factors only slightly decrease the term $\sim f$ and thus the overall zipping rate.

From equation (15), a simple expression for the characteristic alignment time τ_0 can be obtained. For this purpose we assume small angles and linearize equation (15) with respect to ϕ. Assuming that the collective effects are dominating over the change in angle induced by the movement of the intersection point S_0, one obtains

$$\tau_0 = \frac{\eta_r}{2\kappa D} \frac{p_d^2}{p_a}. \tag{18}$$

This estimate is in good agreement with the numerical results discussed in Section 3 and shown in Figure 3, namely that $\tau_0 \propto p_d^2/p_a$ and $\tau_0 \propto 1/D$. Making use of equation (6) and introducing the average motor run length, $l_m = V/p_d$, and the average number of motors attached to both filaments, $N = p_a/p_d$, one can rewrite equation (18) as

$$\tau_0 \simeq \frac{\eta_r}{r d \kappa N l_m}. \tag{19}$$

These parameters are more easily accessible experimentally. For the parameter values given above (resulting in $N \simeq 5$–10 and $l_m \simeq 1\,\mu$m) one obtains $\tau_0 \simeq 5$–10 s. This alignment time is faster by at least one order of magnitude than the alignment by passive crosslinks, reported to be in the order of several minutes [15].

5 Single motor cooperating with a static crosslink

Our formalism also allows for the investigation of another mode of fast alignment, namely by moving motors cooperating with a static crosslink [35]. When the crosslink is attached to both filaments, the intersection point S_0 will not be displaced in the course of alignment and will act as a hinge. In this case, a single motor (with coordinate S_1) leads to fast zipping. Thus, we will focus here only on this simple situation. Equations (2, 3) and (8) then reduce to two equations

$$\partial_t \phi = -\frac{\kappa}{\eta_r} S_1^2 \cos\phi \sin\phi,$$
$$\partial_t S_1 = V(1 - \kappa S_1 \sin^2\phi / F_m). \tag{20}$$

They can be easily solved in two cases, in the limits of either large or small stall forces. For the case of a large stalling force, the motor proceeds with a constant speed like $S_1 \simeq Vt$, and one obtains the characteristic alignment time

$$\tau_0^{cl} = \left(\frac{3\eta_r}{V^2\kappa}\right)^{1/3}, \tag{21}$$

which evaluates to $\simeq 0.3$ s for the parameters as given above. In the limit of a small stall force, the motor is nearly stalled, $\partial_t S_1 \approx 0$, resulting in $S_1 = F_{st}/(\kappa \sin^2\phi)$. The characteristic alignment time then reads

$$\tau_0^{cl} = \frac{\kappa\eta_r}{4F_{st}^2} \tag{22}$$

and amounts to $\simeq 0.4$–1 s.

In conclusion, zipping is very fast if both a crosslink and a motor are involved. Thus, as will be discussed in the experimental part and shown in Figure 6, in order to distinguish experimentally the collective alignment by motors, resulting in the alignment time given by equation (18), from the alignment by cooperation of crosslink-motor pairs, resulting in equations (21, 22), it is important to verify that both microtubule-motor contacts are indeed mobile.

6 Experimental demonstration

To demonstrate fast collective alignment, we performed *in vitro* experiments in a similar geometry: a bead assay was investigated as described previously [19]. Taxol stabilized microtubules were deposited onto poly-L-lysine incubated glass slides. Freely floating microtubules were washed out and the slides were subsequently blocked by casein buffer to prevent nonspecific bead binding.

Carboxylated polystyrene beads (200 nm diameter; Polysciences, Warrington, PA) were incubated with kinesin-1 motors (0.9 nM) and then injected into the flow cells. At this concentration, the beads spontaneously bound to and moved along glass-bound microtubules ($> 15\,\mu$m long). The beads had a very long ($> 8\,\mu$m) run length. Since for individual motors the average travel distance is about $1\,\mu$m, this suggests that the surface of the beads was decorated with a high density of kinesin motors.

In this assay we observed frequent spontaneous binding of beads and microtubules and long-range movement of these beads along microtubules. Most microtubules in our assay are immobilized very tightly on the surface of the glass slide. However, we occasionally found loose microtubules, some of which were linked to stationary ones via the beads. In such cases we observed linear transport of the loose microtubule along the immobilized one. On occasions when the link between microtubules consisted of more than one bead, we could observe zipping events. The loose microtubule is not always easily resolvable in our videos, however the case reported here is representative of the time scale for such events in our assay.

A select time series of such an alignment event is shown in Figure 5A-C, where one microtubule is fixed to the substrate and another, mobile one is connected to the former by the multiple-motor-covered beads. The mutual angle between the microtubules as a function of time is shown in Figure 5D. The alignment time is found to be about 5 s, in qualtitative agreement with the prediction.

As discussed above in the context of the combined action of motors and a crosslink, to make sure that we are probing the collective effects of multiple motors, it is important to verify that all the beads involved are moving. Our setup allows to detect the movements of different beads independently, cf. Figure 6. There, initially the two attachment points are almost at the same location, resulting in minimal zipping force. Due to limits of optical resolution, they cannot be imaged separately first. However, as the process progresses, they move apart so that both beads can be individually tracked. At that point, due to their increased separation, the zipping force has increased, resulting in the decrease in the angle between the microtubules. By tracking each attachment point separately, one clearly sees that both points are moving, though at different speeds, proving that neither attachment point is stationary.

7 Conclusions

In conclusion, we have shown that multiple motors may work together in order to align polar filaments, thus constituting an important precursor of bundle formation. A micromechanical model has been proposed, exhibiting that motors attached to both filaments are localized around the intersection point of microtubules, propagate with a velocity close to the single-motor velocity and result in fast zipping. The average number of attached motors as

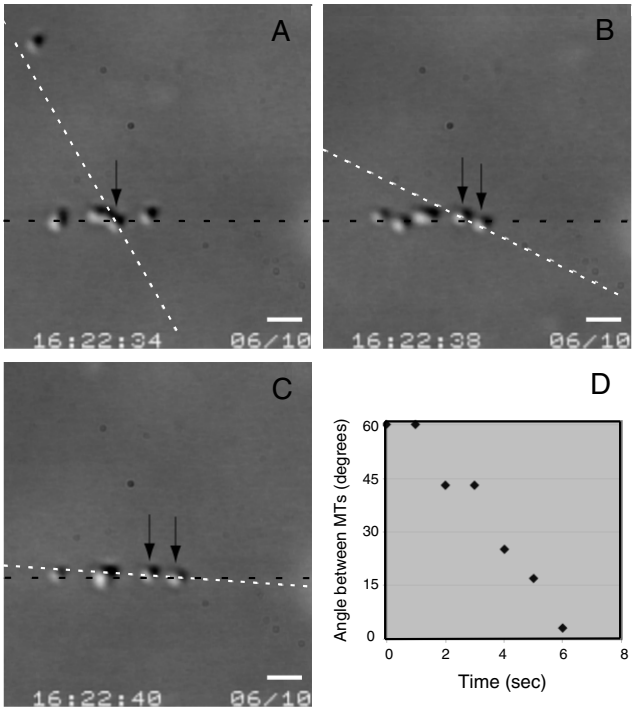

Fig. 5. Two microtubules "zip" together due to multiple motor activity. (A-C): a sequence, showing one microtubule (black dashed line) fixed on a glass slide with a second mobile microtubule (white dashed line) bound to the fixed one via cargos (200 nm diameter polystyrene beads) carrying multiple kinesin-1 motors. Panel D shows the overall angle $\psi = 2\phi$ between the microtubules as a function of time, starting at $\simeq 60°$. The microtubules become almost perfectly aligned within 6 seconds, though the actual zipping took approximately 5 seconds. Times are 0 s, 4 s, and 6 s for A-C, respectively. The scale bar is 1 μm.

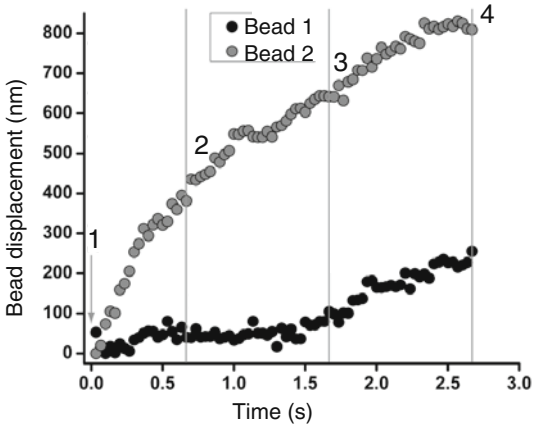

Fig. 6. Verification of the simultaneous motion of both involved beads attached to the microtubules. By tracking each bead separately, possible after the arrow indicated with "1", one clearly sees that both attachment points are moving. The decrease in the angle between the two microtubules is also indicated and evaluates to $\psi = 2\phi = 37°$, $25°$, $17°$ and $3°$ for the sample points indicated by the vertical bars, 1 to 4.

well as the randomness of the motor stepping appear to be the most important parameters determining the alignment time. The proposed model has been also used to account for the case of motors and crosslinks. It could also be generalized to the possible case where two populations of motors walking in opposite directions are present.

In the situation of multiple motors interacting with a pair of filaments studied here, a force-velocity relation has only quantitative effects, in contrast to, *e.g.*, multiple motors pulling a tube from a membrane [22]. Also a force dependence in the detachment rate leads only to quantitative changes. Both effects, as one would expect, slow down the zipping, but only for appreciable initial angles and in the limit of a small number of motors. Remarkably, the motor clustering near the intersection point *does not* rely on direct interaction between the motors (*e.g.*, excluded volume or effects of hydrodynamic coupling) and is thus different from mechanisms based on asymmetric exclusion processes [36]. It also differs from zipping by successive attachment of nonprocessive motors to soft actin filaments as reported in reference [17]. The effective attraction of the motors is solely due to the fact that their extension is coupled globally through the mutual angle of the microtubules.

Together with the experimental demonstration of the fast alignment process, our work suggests another interesting example where motors efficiently achieve a desired goal by working together. Clearly more detailed experiments are needed to validate our predictions. The most convincing test would be to measure directly the temporal dependence of the angle, however obtaining sufficient statistics requires a large amount of experimental data which is not easy to achieve. Several indirect aspects of the alignment dynamics could be clarified more easily by using multiheaded motors like Eg5 [18], kinesin-14 or artificial oligomers as in reference [4] instead of motor-covered beads. Labeling the motors should reveal an increased density of motors near the intersection point. The predicted scaling for the alignment time could be verified, for example, by varying the ATP concentration, which in turn controls the motor run length l_m, the motor speed, and the average number of motors attached to the tubules N.

Our theory is built on the assumption that all motors are mobile in the course of alignment. The presence of a nonmoving motor (*e.g.*, a defective one, not able to convert ATP) —or of a crosslink— changes the scaling of the alignment time, as discussed in Section 5. The need to clearly separate these two modes of zipping constitutes another example where *in vitro* experiments are of valuable use to clarify more complex situations *in vivo*. It is quite likely that multiple motors align filaments much faster than crosslinks alone, since the latter have to diffuse towards the intersection point and to successively attach, thereby causing gradual changes in the mutual orientation. Reference [15] seems to confirm that the time scale of crosslink-induced alignment is of the order of minutes. However, some crosslinks (*e.g.* fascin, which is associated to actin) favor parallel orientation and might induce faster alignment. To study *in vitro* the alignment by crosslinks is a worthwhile study, as is the cooperation of crosslinks and motors, that has been predicted here to lead to very

fast alignment. Indeed, as this cooperation is the fastest mode of alignment, suggested by our modeling, it might be beneficial for the cell to make use of *both* crosslinks and motors in order to efficiently align filaments.

We thank Stefan Diez, David Lacoste, George Shubeita and Lev Tsimring for useful discussions. F.Z. and I.S.A. acknowledge support by the US DOE, grant DE-AC02-06CH11357, S.P.G. by the NIH Grant 1RO1GM070676 and M.V. by the NIH Ruth L. Kirschstein National Research Service Award postdoctoral fellowship.

Appendix A.

The quasi-stationary Fokker-Planck equation for the probability distribution function of the motors, equation (14), in the absence of force-dependent effects reads

$$0 = D\partial_{\tilde{S}}^2 P - \delta V \partial_{\tilde{S}} P - (p_d - \alpha)P + p_a \delta(\tilde{S}), \qquad (A.1)$$

with $\delta V = V - \dot{S}_0$ and $\alpha = V\kappa \sin^2\phi / F_{st}$. One obtains exponential solutions $P_{l,r} = a_{l,r} e^{V_\pm S}$, where l, r refer to the solutions to the left and right of the intersection point $\tilde{S} = 0$, with

$$V_\pm = \frac{1}{2D}\left[\delta V \pm \sqrt{\delta V^2 + 4p_d D}\right]. \qquad (A.2)$$

Here we have already used that the probablity to have motors far from the intersection point should vanish. To determine a_l and a_r we need two conditions: first, the continuity of the probability at the intersection point, $P_l(0) = P_r(0)$, and second a jump condition for the derivative implied by the δ-function in equation (A.1), $V_p P_l(0) - V_m P_r(0) = p_a/D$.

Inserting the obtained solution into equations (12, 13) and integration leads to two effective equations for the angle of the microtubule pair and the intersection point

$$\dot{\phi} = \frac{\kappa}{\eta_r} \cos\phi \sin\phi \, \Phi(S_0, \delta V), \qquad (A.3)$$

$$\dot{S}_0 = -\frac{\kappa}{\eta_r} \cos^2\phi S_0 \, \Phi(S_0, \delta V) + \frac{\kappa}{\eta_t} \frac{p_a}{p_d^2} \delta V, \qquad (A.4)$$

with

$$\Phi(S_0, \delta V) = -\frac{p_a}{p_d^2}\left[2D + S_0 \delta V + \frac{2}{p_d}\delta V^2\right]. \qquad (A.5)$$

The right-hand sides of equations (A.3, A.4) contain $\dot{S}_0$ via δV. However, the quadratic term in δV occurring in $\Phi(S_0, \delta V)$ can be safely neglected, since the speed of the intersection point $\dot{S}_0$ is very close to V. This has been verified numerically and it is also clear from the fact that the intersection point remains close to the position of all motors at any time. Then equation (A.4) can be solved for δV, leading to

$$\delta V = V - \dot{S}_0 = \frac{V - 2\frac{\kappa}{\eta_r}\frac{p_a}{p_d^2}\cos^2\phi \, D S_0}{1 + \frac{\kappa}{\eta_r}\frac{p_a}{p_d^2}\cos^2\phi S_0^2 + \frac{\kappa}{\eta_t}\frac{p_a}{p_d^2}}. \qquad (A.6)$$

Neglecting the 1 in the denominator ($1 \ll \frac{\kappa}{\eta_t}\frac{p_a}{p_d^2} \simeq 5000$ holds for the parameters given above), by insertion into equation (A.3) one arrives at

$$\dot{\phi} = -\cos\phi \sin\phi \frac{\tilde{\eta}\left(VS_0 + 2D\frac{\kappa}{\eta_t}\frac{p_a}{p_d^2}\right)}{1 + \tilde{\eta}\cos^2\phi S_0^2}, \qquad (A.7)$$

which is equation (15) with $f = p_a/p_d^2$.

In case the motors' speed is load-dependent, although the homogeneous part of equation (14) has an analytical solution in terms of confluent hypergeometric functions, this solution is impractical to proceed with. By the substitution $P(\tilde{S}) = \exp\left(\frac{\delta V}{2D}\tilde{S} - \frac{\alpha}{4D}\tilde{S}^2\right)\bar{P}(\tilde{S})$, we transform equation (14) to the form without first derivative,

$$\partial_{\tilde{S}}^2 \bar{P} - \left(\frac{p_d - \alpha/2}{D} + \frac{(\delta V - \alpha\tilde{S})^2}{4D^2}\right)\bar{P} + p_a \delta(\tilde{S}) = 0. \qquad (A.8)$$

For not too high value of α, the second term in the bracket can be dropped compared to the first one. To be more specific, for $\alpha \to 0$ and $p_d \sim O(1)$ this approximation invalidates when $(\alpha\tilde{S})^2/D \approx p_d$. However, due to the factor $\exp[-\alpha\tilde{S}^2/4D]$, the function $P(\tilde{S})$ becomes exceedingly small because $\alpha\tilde{S}^2/D \approx p_d/\alpha \gg 1$. Upon the neglection of the second term in the bracket, the function $P(\tilde{S})$ can be obtained again, and one can proceed in analogy to the previous case.

References

1. H. Lodish *et al.*, *Molecular Cell Biology* (W. H. Freeman, New York, 1999).
2. K. Takiguchi, J. Biochem. **109**, 520 (1991).
3. R. Urrutia, M.A. McNiven, J.P. Albanesi, D.B. Murphy, B. Kachar, Proc. Natl. Acad. Sci. U.S.A. **88**, 6701 (1991).
4. F.J. Nédélec, T. Surrey, A.C. Maggs, S. Leibler, Nature **389**, 305 (1997).
5. T. Surrey, F. Nédélec, S. Leibler, E. Karsenti, Science **292**, 116 (2001).
6. D. Smith, F. Ziebert, D. Humphrey, C. Duggan, M. Steinbeck, W. Zimmermann, J. Käs, Biophys. J. **93**, 4445 (2007).
7. K. Kruse, J.F. Joanny, F. Jülicher, J. Prost, K. Sekimoto, Phys. Rev. Lett. **92**, 078101 (2004).
8. I.S. Aranson, L.S. Tsimring, Phys. Rev. E **74**, 031915 (2006).
9. F.C. MacKintosh, A.J. Levine, Phys. Rev. Lett. **100**, 018104 (2008).
10. H. Nakazawa, K. Sekimoto, J. Phys. Soc. Jpn. **65**, 2404 (1996).
11. K. Kruse, F. Jülicher, Phys. Rev. E **67**, 051913 (2003).
12. R. Peter, V. Schaller, F. Ziebert, W. Zimmermann, New J. Phys. **10**, 035002 (2008).
13. M.M.A.E. Claessens, M. Bathe, E. Frey, A.R. Bausch, Nature Mater. **5**, 748 (2006).
14. O. Lieleg, M.M.A.E. Claessens, C. Heussinger, E. Frey, A.R. Bausch, Phys. Rev. Lett. **99**, 088102 (2007).
15. D. Vignjevic, D. Yarar, M.D. Welch, J. Peloquin, T. Svitkina, G.G. Borisy, J. Cell Biol. **160**, 951 (2003).

16. J. Kierfeld, J.T. Kühne, R. Lipowsky, Phys. Rev. Lett. **95**, 038102 (2005).
17. J. Uhde, M. Keller, E. Sackmann, A. Parmeggiani, E. Frey, Phys. Rev. Lett. **93**, 268101 (2004).
18. L.C. Kapitein, E.J.G. Peterman, B.H. Kwok, J.H. Kim, T.M. Kapoor, C.F. Schmidt, Nature **435**, 114 (2005).
19. M. Vershinin, B.C. Carter, D.S. Razafsky, S.J. King, S.P. Gross, Proc. Natl. Acad. Sci. U.S.A. **104**, 87 (2007).
20. M. Doi, S.F. Edwards, *The Theory of Polymer Dynamics* (Clarendon Press, Oxford, 1986).
21. S. Klumpp, R. Lipowsky, Proc. Natl. Acad. Sci. U.S.A. **102**, 17284 (2005).
22. O. Campás, Y. Kafri, K.B. Zeldovich, J. Casademunt, J.-F. Joanny, Phys. Rev. Lett. **97**, 038101 (2006).
23. K. Visscher, M.J. Schnitzer, S.M. Block, Nature **400**, 184 (1999).
24. C.M. Coppin, D.W. Pierce, L. Hsu, R.D. Vale, Proc. Natl. Acad. Sci. U.S.A. **94**, 8539 (1997).
25. A. Parmeggiani, F. Jülicher, L. Peliti, J. Prost, Europhys. Lett. **56**, 603 (2001).
26. S.W. Grill, K. Kruse, F. Jülicher, Phys. Rev. Lett. **94**, 108104 (2005).
27. C.M. Coppin, J.T. Finer, J.A. Spudich, R.D. Vale, Biophys. J. **68**, 242s (1995).
28. F.J. Nédélec, J. Cell Biol. **158**, 1005 (2002).
29. F. Ziebert, I.S. Aranson, Phys. Rev. E **77**, 011918 (2008).
30. F. Gittes, B. Mickey, J. Nettleton, J. Howard, J. Cell Biol. **120**, 923 (1993).
31. D. Karpeev, I.S. Aranson, L.S. Tsimring, H.G. Kaper, Phys. Rev. E **76**, 051905 (2007).
32. H. Risken, *The Fokker-Planck Equation* (Springer, Berlin, 1989).
33. To simplify the integrals, in analytical calculations we extended the limits of integration to infinity. We verified that this leads only to small quantitative changes.
34. The complete dependence reads ($\zeta = p_d - \alpha/2$)

$$f(\alpha) = -\frac{2p_a}{\alpha^2}\left[1 - \frac{\sqrt{\pi}p_d}{\sqrt{\alpha\zeta}}\exp\left(\frac{\zeta}{\alpha}\right)\mathrm{erfc}\sqrt{\frac{\zeta}{\alpha}}\right].$$

35. F. Ziebert, I.S. Aranson, L.S. Tsimring, New J. Phys. **9**, 421 (2007).
36. A. Parmeggiani, T. Franosch, E. Frey, Phys. Rev. Lett. **90**, 086601 (2003).